

# Axial Ratio Bandwidth Enhanced Proximity Fed Fractal MGS-Based Circularly Polarized Patch Antenna

Ramya Radhakrishnan\* and Shilpi Gupta

**Abstract**—A triangle-shaped proximity-fed circularly polarized antenna with a modified fractal ground structure is introduced in this paper. The antenna’s ground plane is employed with a fractal-shaped corporate feed type cut, which helps produce the circular polarization. The proximity feed is offset from the center to generate the orthogonal modes; furthermore, the fractal modified ground aids in enhancing the axial ratio bandwidth. Different iterations of the basic fractal unit improve the polarization purity and axial ratio bandwidth. The experimental results of the designed antenna reflection coefficients below 10 dB at 2.5 GHz show an impedance bandwidth of 260 MHz (2.35 GHz to 2.61 GHz) and axial ratio bandwidth of 120 MHz (2.48 GHz to 2.60 GHz). The simulated and measured results show a good agreement.

## 1. INTRODUCTION

The technological advancement in the sectors like IoT, 5G, and various health care has seen exponential growth in the development of wireless devices in the past few years. The use of circularly polarized (CP) antennas has increased due to the need to communicate irrespective of receiver alignment and vital communication links [1]. State of the art implies various methodologies to generate circular polarization that includes perturbation in the patch [2], adding a plus-shaped slot or slit [4], corner truncation [5], adding tabs, etc. In the context of triangular patch antennas, CP can be relatively easily achieved by adding a tuning stub [6] at the tip and center of one of the sides, a Y-shaped slot [7], spur lines [8], a cross-slot [9], and tip truncation [10]. Besides the single feed where the patch currents can be modified by perturbing the patch dimensions, dual-feed methods use power dividers to produce CP. Its exceptional ability to combat multipath interference, reduction in effects due to Faraday rotation, and robustness to the misalignment see its applications in Multiple Input Multiple-Output (MIMO) systems, satellite communications, and mobile devices. Over the last few decades, fractal antennas have gained popularity due to their ability to improve the bandwidth and make the antennas compact. Benoit Mandelbrot coined the word “fractal” to acknowledge “roughness and self-similarity”. The letter presented in [11] depicts an innovative method for designing a single feed CP microstrip antenna with Fractal Defected Ground Structure (FDGS). This strategy not only produces circular polarization but also improves the cross-polar levels. The second and third iterative CP microstrip antennas significantly improved achieving CP. The circular patch of CP radiation is imprinted with two asymmetric length rectangular-shaped slots perpendicular to each other. Koch’s fractal DGS in [12] aids size reduction by 44.74%, improved bandwidth of AR by 62.73%, impedance bandwidth by 70.74%, and radiation effectiveness by 4.03% compared to conventional patch antennas. A 90° flare angular sector-shaped broadband antenna is depicted in [13]. The paper in [14] describes a stacked antenna with fractal DGS contributing to size reduction and multi-band operation. Square notches on the side lengths contribute to the tuning and bandwidth improvement of the axial ratio. The same element, stacked as a parasitic patch with 0.8 mm

---

*Received 10 May 2022, Accepted 20 July 2022, Scheduled 7 August 2022*

\* Corresponding author: Ramya Radhakrishnan (d18ec001@eced.svnit.in).

The authors are with the Sardar Vallabhbhai National Institute of Technology, Surat, India.

height substrate material, improved the gain considerably. A single feed E-shaped patch with inclined fractal defected ground structure (IFDGS) is proposed in this article [15]. Like the traditional patches that use notches to generate CP in [13], a similar idea has been implemented to produce CP with sector patches. Some miniaturization was achieved, and the design was extended to make an array of patches to improve the gain. It is evident from the experimental results that this strategy significantly enhanced the impedance bandwidth, axial ratio (AR) bandwidth, and antenna gain. The work depicted in [16] is a slot antenna loaded with parasitic patches to obtain a maximum usable CP bandwidth. An inclined FDGS has been discussed in [17] and [15]; the fractal DGS is achieved in the ground plane inclined along the diagonal axis. The work in [18] gives a detailed understanding of the fractal structure used in the paper with a square patch. A unified design defected ground structure, U-shaped branches, folded stepped impedance stubs, and window-shaped radiation patch slots help increase the impedance bandwidth and resonance frequency [19]. Additionally, the decoupling structure designed aids in improving the isolation among the adjacent MIMO antennas. The generation of the degenerate modes with an in-depth analysis with the help of resonant curves and current distributions is clearly explained. A CP equilateral triangle for synthetic aperture radar proposed in [21] describes a dual-feed proximity coupling to generate CP. The power divider helps obtain the  $90^\circ$ -phase difference between the orthogonal components. A CP-modified isosceles triangular patch antenna described in [22] is realized by overlapping two triangular patch antennas. Here the near degenerate modes are excited by the offset distance and the inter-spacing between them. A radiation pattern restoration-based polarization diversity CP antenna is proposed in [20]. Here the antenna works in dual-polarization, i.e., LHCP and RHCP with the former used for transmission and the latter for reception.

The proposed work attempts to attain circular polarization using a corporate feed type MGS. The former helps in exciting the degenerate modes, and a triangular patch is a proximity feed to excite the CP. The primary focus was to use maximum CP usable bandwidth from the obtained impedance bandwidth. Henceforth, an offset feed is provided in the second stage of antenna design to aid a phase difference of  $90^\circ$ . Furthermore, the added structure from [11] was placed parallel to the E-field orientation to alter the surface current distributions at  $135^\circ$  and  $225^\circ$  to impart extra axial ratio bandwidth. The latter helps improving the usable CP bandwidth increasing the surface current lengths. The technical aspects are conferred in four parts. The first part links a brief introduction to the state of the art and the motto of the work. The antenna design and mathematical modeling are discussed in the second part. Later, the third part mentions a brief parametric analysis and surface current distributions, followed by simulated results in part four.

## 2. ANTENNA CONFIGURATION AND DESIGN METHODOLOGY

Figure 1 shows the fabricated antenna prototype, a proximity-fed triangular patch antenna with a modified ground structure. Figure 2 illustrates the designed antenna geometry, an equilateral triangle

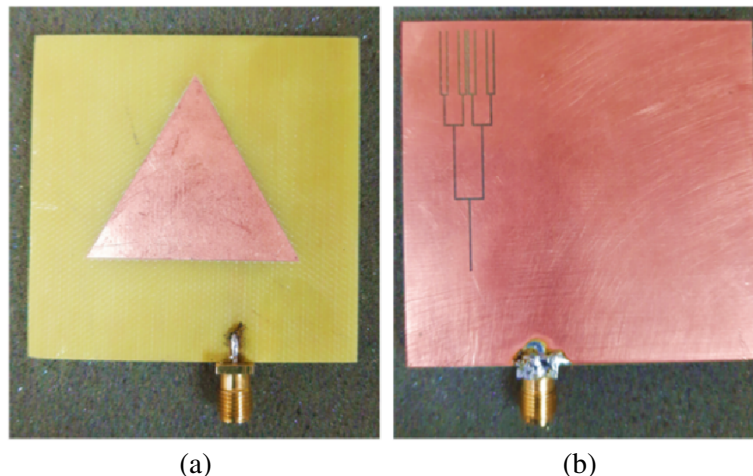


**Figure 1.** (a) Top view of the fabricated antenna. (b) Bottom view of the fabricated antenna.

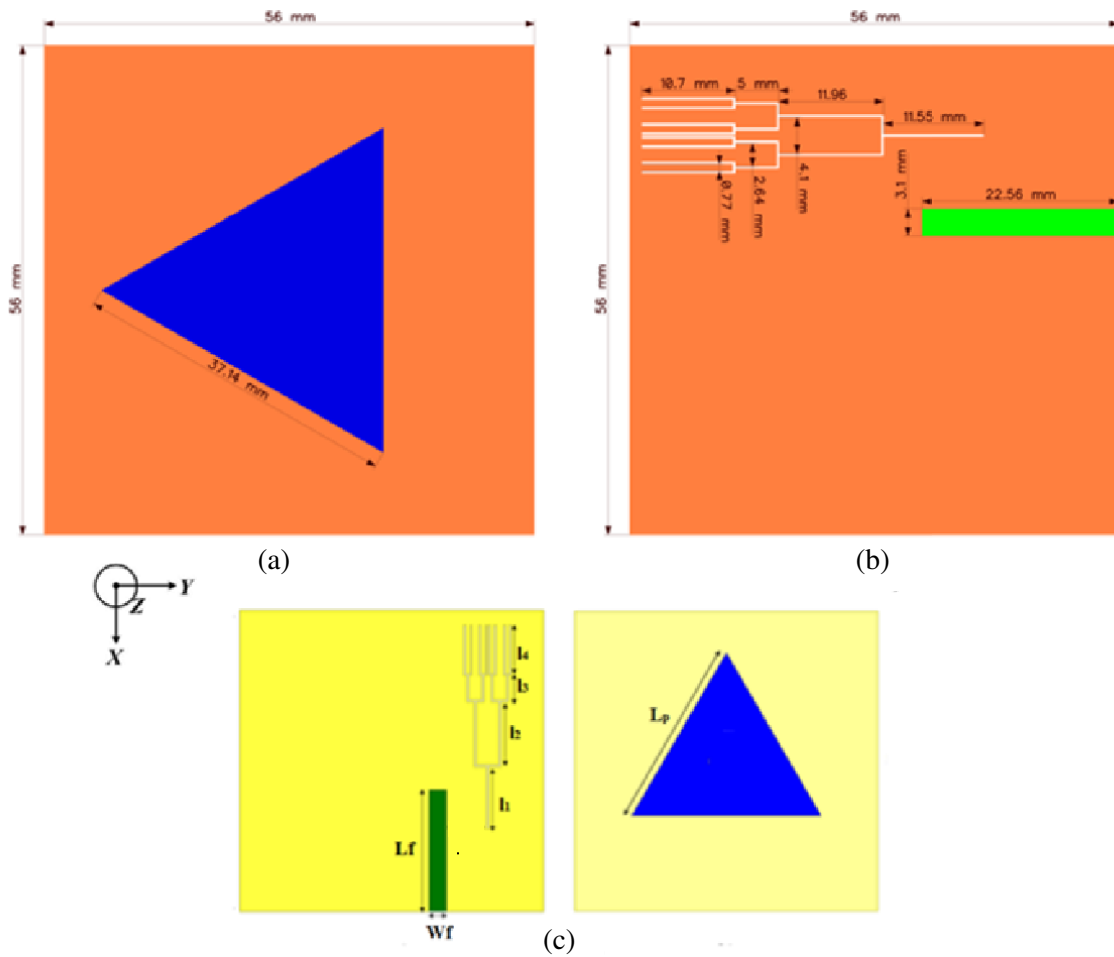


**Figure 2.** (a) Top view of the patch on substrate 1. (b) Top view of the proximity feed on substrate 2. (c) Geometry and dimensions of the fractal MGS and patch.

with the side  $L = 37.14\text{ mm}$  in length, and the heights of substrate 1 and substrate 2 are  $1.6\text{ mm}$ . The triangular patch lies on an FR4 substrate of thickness  $h$  and relative permittivity  $\epsilon_r$ , fed with a proximity feed of size  $L_f$  and  $W_f$ . The ground plane with dimensions length ( $L_g$ )  $\times$  width ( $W_g$ ) has a corporate feed structure cut that additionally provides the phase difference, increasing the current lengths. Near degenerate modes with the same amplitudes and  $90^\circ$  out of phase, components are excited by slightly making the cross slot and offsetting the feed from the center. The improved ground structure also increases the surface currents, aiding bandwidth enhancement. The design is modeled in Ansys High-Frequency Structure Simulator [23]. However, a left-hand circularly polarized antenna can be obtained by changing the ground’s feed and slot structure to the left side.

### 2.1. Mathematical Modeling of the Designed Antenna

A simple triangular proximity-fed patch antenna has been modeled in the first stage, and its odd and even symmetric modes are observed. Further, the feed has been offset from the center to achieve a right-hand circularly polarized antenna. The axial ratio bandwidth was observed to be small; another modified ground structure in [11] has been added to enhance it. Upon carrying out a brief parametric analysis, the modified fractal ground structure helped improve the axial ratio bandwidth of the proximity-fed patch antenna. The optimized antenna parameters are depicted in Table 1, and Figure 2 approximates and improves using the equation below. The dimensions of the triangular patch on the substrate for

**Table 1.** Optimized dimensions of the proposed antenna.

Parameter	$L$	$L_f$	$W_f$	$l_1$	$l_2$	$l_3$	$l_4$	$w_1$	$w_2$	$w_3$	$L_g$	$W_g$	$d$
Value (mm)	35.14	22.5	3.1	11.5	11.96	5	10.7	4.1	2.64	0.77	56	56	7.5

TM<sub>10</sub> are compared by using the following equation [3]

$$L_p = \frac{2c}{f_0 \sqrt{\epsilon_r}} \sqrt{m^2 + n^2 + mn} \quad (1)$$

where,

$L$  = Length of the patch,

$c$  = Speed of light,

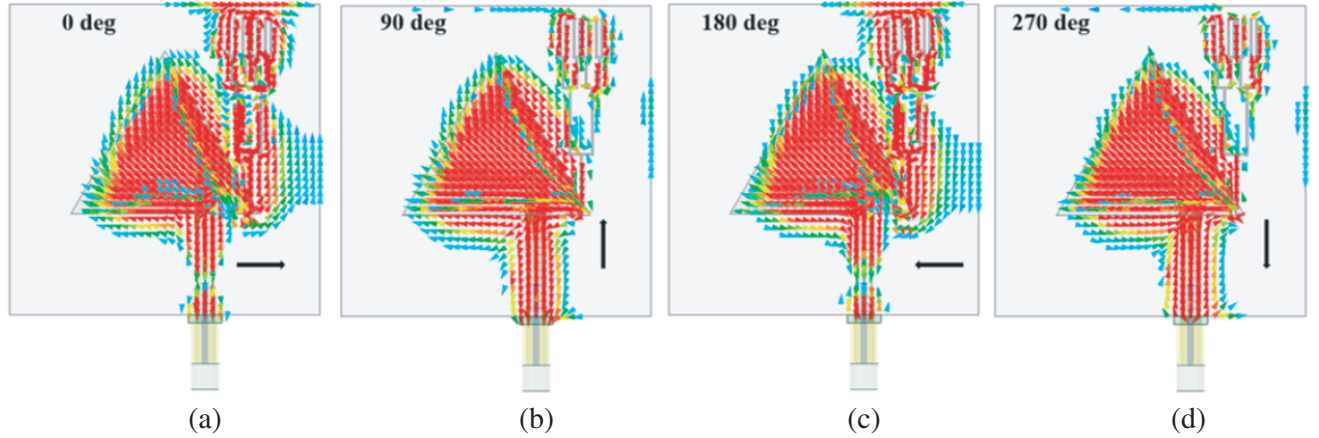
$\epsilon_r$  = Dielectric constant,

$f_0$  = Resonant frequency,

$m, n$  are the half-cycle variations.

## 2.2. Surface Current Distributions

The surface current distributions of the modeled antenna at 2.5 GHz are illustrated in Figure 3. For various rotation angles with a step size of 90°, the orientation of the fields shows a counterclockwise rotation. The antenna is simulated in Ansys HFSS in the  $XY$  plane, where the direction of the propagation is towards the positive  $Z$  direction, indicating Right Hand Circular Polarization. The odd and even symmetric modes TM<sub>10</sub> and TM<sub>01</sub> are excited, indicating the maximum fields concentrated around the lower right vertex. The former led to the placement of MGS beneath the vertex to provide extra current length path and phase, aiding in perfectly exciting the degenerate modes. It is observed that at 135° and 225° the various angles of rotation of surface currents are altered thereby making it rotate anticlockwise.

**Figure 3.** Vector surface current distributions at 2.5 GHz.

## 2.3. Effects of Different Parameters on the Antenna

The design's functional variables were subjected to a thorough parametric study. The parameters are modified once, with the others held constant, to determine their effect on the return loss characteristics. Furthermore, multiple parameters are also analyzed by considering two parameters simultaneously to optimize the design to attain better stability in terms of axial ratio. Table 1 shows the optimum parameters for the proposed antenna.

2.3.1. Effect of  $l_1$  on Reflection Coefficient and Axial Ratio

The modified fractal ground structure, an iterative U structure, contributes to the circular polarization. Figure 4 illustrates the effects of varying  $l_1$  on the reflection coefficient and axial ratio plots with a step size of 0.5 mm. As the value varies from 10.5 mm to 12 mm, the excitation frequency of orthogonal modes fluctuates abruptly. The axial ratio plot depicts the orthogonal mode excitation out of the impedance bandwidth curve at  $l_1 = 11.5$  mm; a perfect overlap of the degenerate modes is obtained at  $l_1 = 11$  mm.

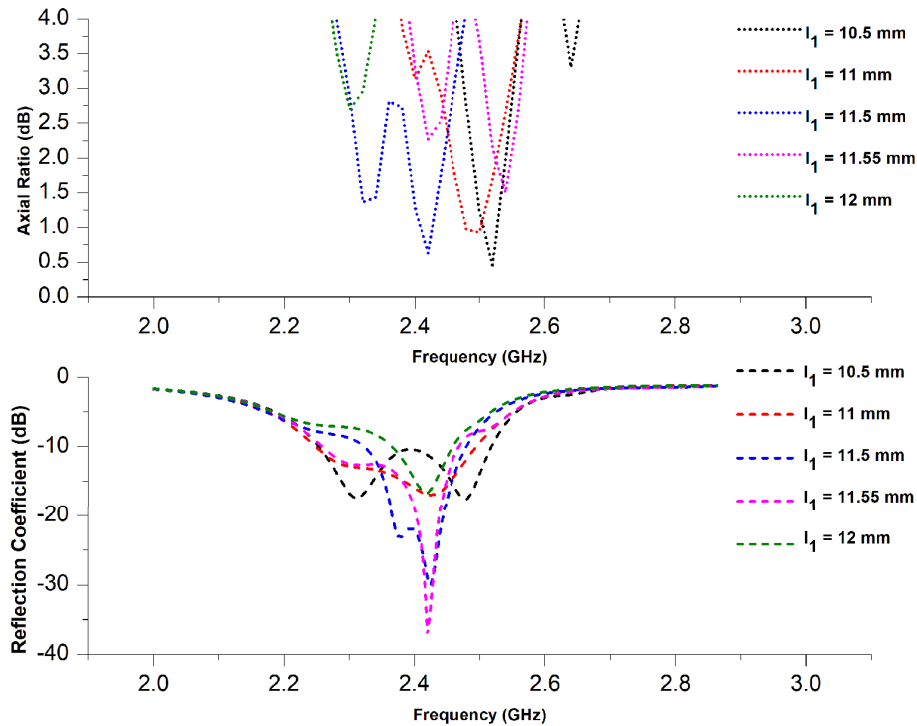


Figure 4. Effect of  $l_1$  on reflection coefficient and Axial ratio.

2.3.2. Effect of  $l_2$  on Reflection Coefficient and Axial Ratio

Figure 5 illustrates the impact of varying  $l_2$  on the  $S_{11}$  (dB) and axial ratio curves. It is evident from the plot that as the value of  $l_2$  increases from 11 mm to 13 mm, the generation of degenerate mode has deteriorated. At  $l_2 = 11.4$  mm, the axial ratio bandwidth curve overlaps with the 10 dB impedance bandwidth curve.

2.3.3. Effect of  $w_2$  on Reflection Coefficient and Axial Ratio

Varying  $w_2$  significantly contributes to the axial ratio bandwidth tuning and improvement. Figure 6 illustrates that though the orthogonal modes are obtained at  $w_2 = 2.85$  mm and 3.15 mm, a perfect overlay of the axial ratio and impedance bandwidth is observed at  $w_2 = 2.85$  mm. At other values of  $w_2$ , the orthogonal modes are not excited at the frequency of interest.

3. RESULTS AND DISCUSSION

Triangle-shaped proximity feed with a modified ground structure is simulated on a low-priced dielectric substrate (FR-4), dielectric constant ( $\epsilon_r$ ) = 4.4, and operating frequency of 2.5 GHz. The design constraints are listed in Table 1. The construction and design model is shown in Figure 1. The results are validated by printing the antenna on a standard PCB prototype machine and testing the

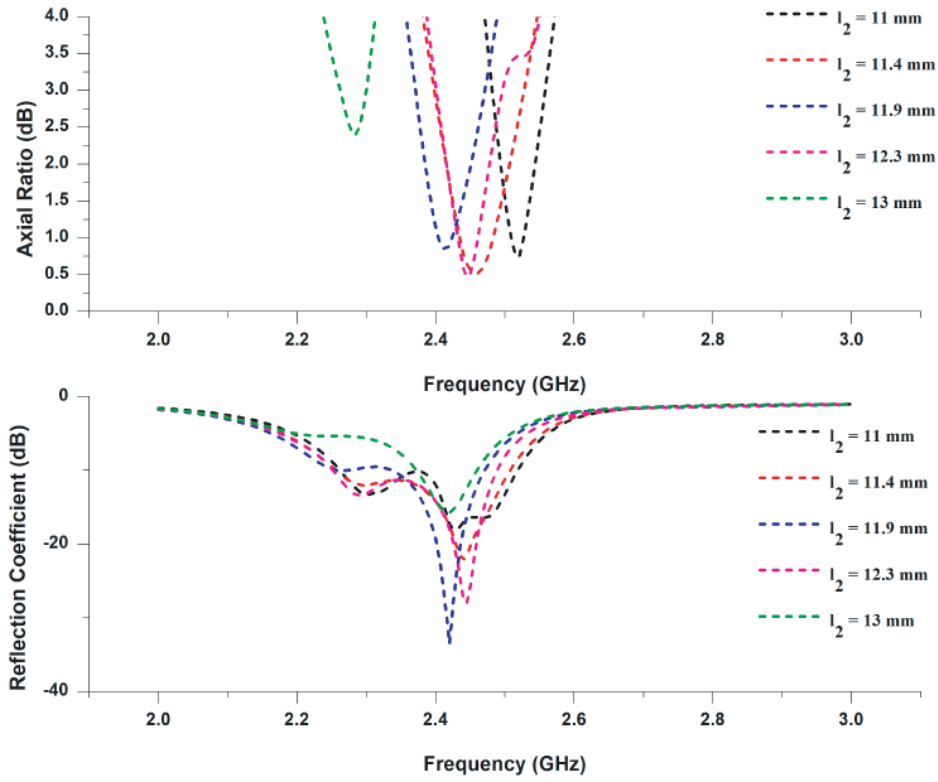


Figure 5. Effect of  $l_2$  on reflection coefficient and Axial ratio.

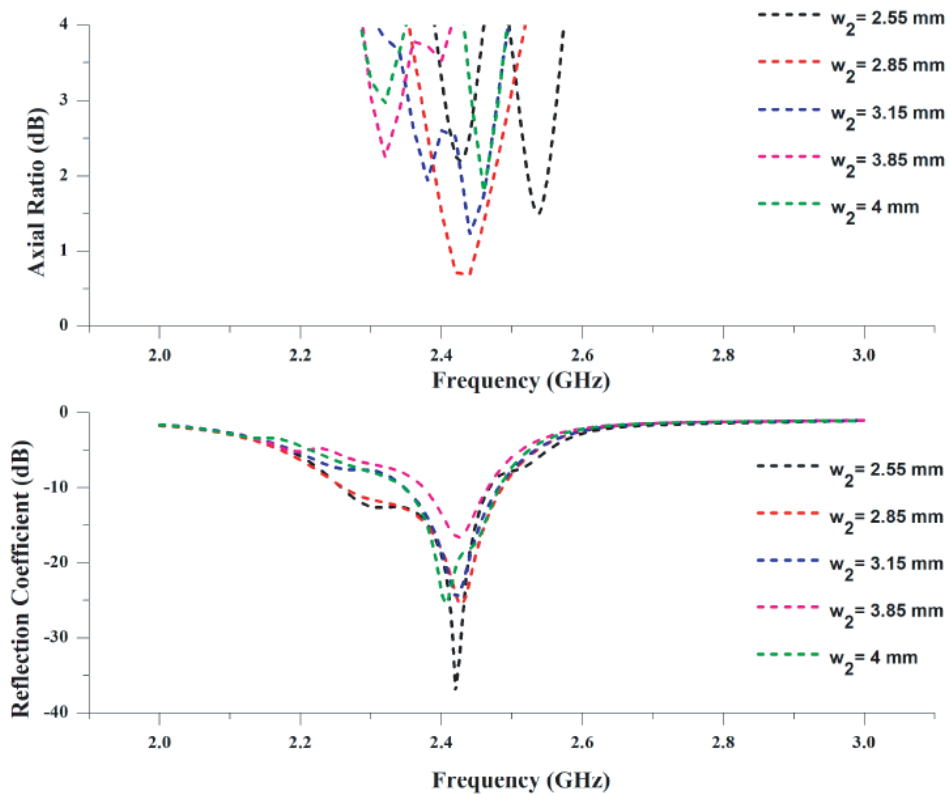


Figure 6. Effect of  $w_2$  on reflection coefficient and Axial ratio.

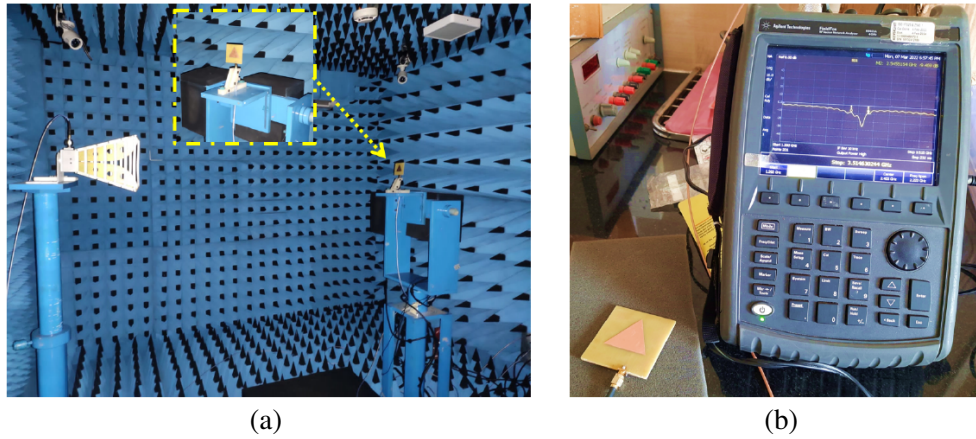


Figure 7. Test and measurement setup anechoic chamber and VNA setup.

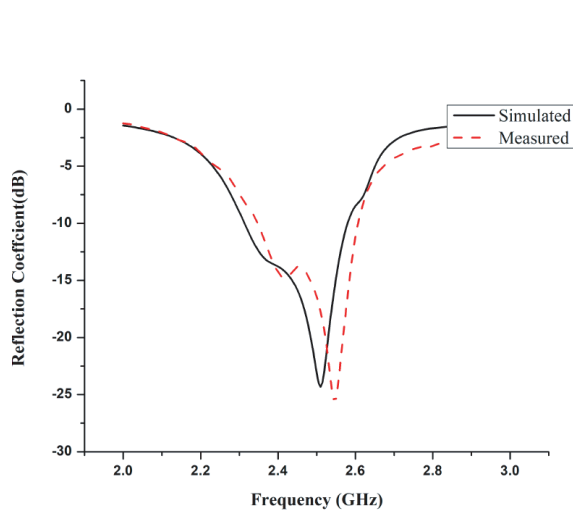


Figure 8. Simulated and measured antenna reflection coefficients.

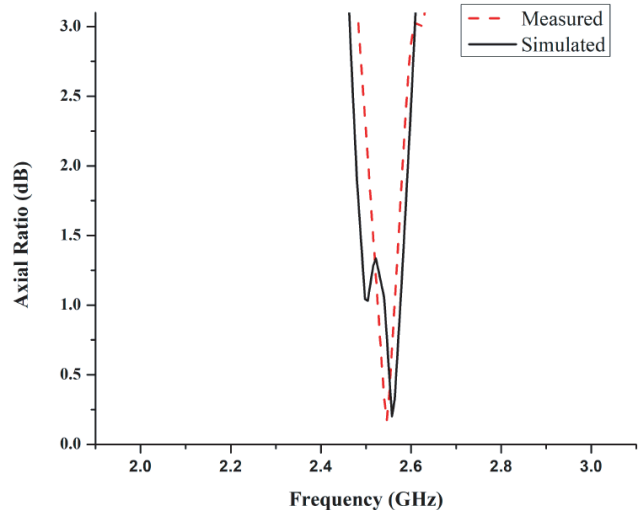


Figure 9. Simulated and measured axial ratio plot.

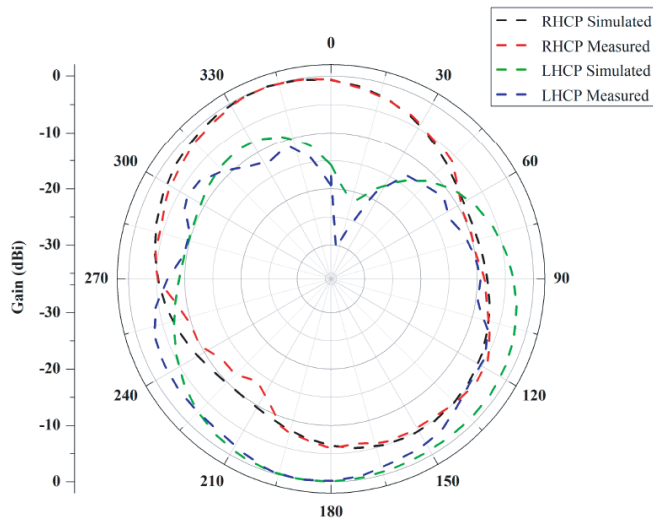
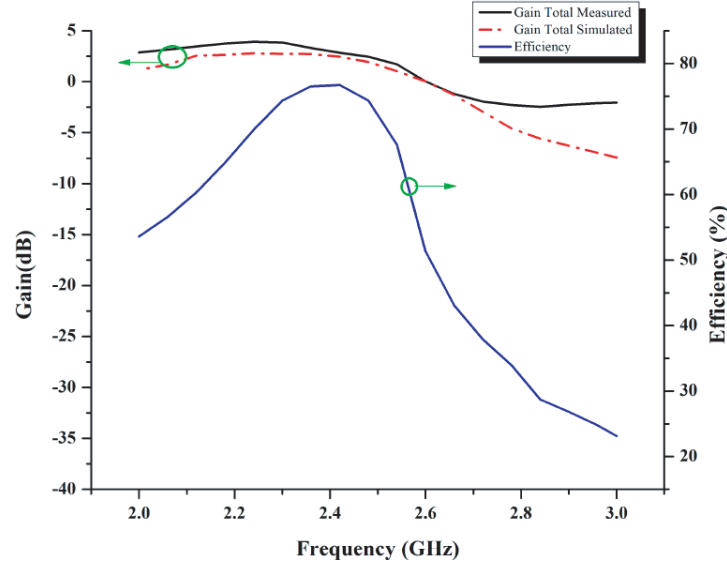


Figure 10. Radiation patterns at 2.5 GHz.



**Figure 11.** Gain vs frequency and efficiency.

same on Agilent TM Vector Network Analyzer connected with an RF anechoic chamber, as shown in Figure 7. Table 2 illustrates a comparison of the designed prototype with the existing state of the art. The simulated and measured reflection coefficients ( $S_{11}$  in dB) are shown in Figure 8. The simulated and measured results show that the reflection coefficients are below 10 dB reference at 2.5 GHz. The reflection coefficient plots of the simulated results show a bandwidth of 260 MHz (2.35 GHz to 2.61 GHz). From Figure 9, it is clear that the axial ratio bandwidth is 120 MHz (2.48 GHz to 2.60 GHz). Figure 10 presents the antenna's RHCP and LHCP radiation patterns. Figure 11 illustrates gain vs frequency and efficiency plots depicting a gain around (2.5–3) dBi in the operating frequency range with an efficiency of 76%.

**Table 2.** Comparison of various parameters for circularly polarized antennas.

Reference	Resonant Frequency/ Band (GHz)	Size (mm <sup>2</sup> )	Impedance Bandwidth (%)	Axial Ratio Bandwidth (MHz)	Polarization
[11]	1.575	100 × 100 × 3.18	6.4	6	RHCP
[15]	3.5	41 × 41 × 1.6	12.7	87	RHCP
[18]	2.81	68 × 68 × 1.6	3.75	32	RHCP
[24]	2.54	36 × 36 × 3.2	6.4	50	LHCP
[25]	2.45	62 × 62 × 1.6	4.5	12	RHCP
[26]	1.65	65 × 65 × 3.18	1.8	10	LHCP
[27]	2.73	54 × 54 × 0.8	1.9	8	LHCP
[28]	1.48	58.7 × 58.7 × 1.6	124.58	68.81	LHCP
[29]	4.1, 5.8, and 6.7	25 × 25 × 1.02	10.3, 9.6, and 12.3	43, 96, 123	RHCP
Proposed Design	2.5	56 × 56 × 3.18	10.5	120	RHCP

#### 4. CONCLUSION

The manuscript presents a simple bandwidth-enhanced triangular-shaped proximity-fed antenna with a modified ground structure that improves axial ratio bandwidth. The fractal modified ground structure aids in improving the polarization purity by exciting the adjacent modes. An RHC polarized antenna with a gain of around 3 dBi is obtained with an impedance bandwidth of 10.48% and axial ratio bandwidth of 4.7%.

#### REFERENCES

1. Toh, B. Y., R. Cahill, and V. F. Fusco, "Understanding and measuring circular polarization," *IEEE Transactions on Education*, Vol. 46, No. 3, 313–318, Aug. 2003.
2. James, J. R., P. S. Hall, and C. Wood, *Microstrip Antenna*, Peter Peregrinus, 1981.
3. Helszajn, J. and D. S. James, "Planar triangular resonators with magnetic walls," *IEEE Transactions on Microwave Theory and Techniques*, Vol. 26, No. 2, 95–100, Feb. 1978.
4. Haneishi, M., T. Nambara, and S. Yoshida, "A design method of circularly polarised rectangular microstrip antenna by one-point feed," *Electronics and communication*, Japan, 1981.
5. Haneishi, M., T. Nambara, and S. Yoshida, "Study on ellipticity properties of single-feed-type circularly polarised microstrip antennas," *IEEE Electronics Letters*, Vol. 18, No. 5, 191–193, 1982.
6. Lu, J.-H. and K.-L. Wong, "Single-feed circularly polarized equilateral-triangular microstrip antenna with a tuning stub," *IEEE Transactions on Antennas and Propagation*, Vol. 48, No. 12, 1869–1872, Dec. 2000.
7. Yang, K. P., K. L. Wong, and J. H. Lu, "Compact circularly polarized triangular microstrip antenna with Y-shaped slot," *Microwave Optical Technology Letters*, 31–34, Jan. 1999.
8. Lu, J. H., H. C. Yu, and K. L. Wong, "Compact circular polarization design of equilateral-triangular microstrip antenna with spur lines," *Electronics Letters*, Vol. 34, 1989–1990, Oct. 1998.
9. Lu, J. H., C. L. Tang, and K. L. Wong, "Single-feed slot-loaded equilateral-triangular microstrip antenna for circular polarization," *IEEE Trans. Antennas Propagat.*, Vol. 47, 1174–1178, Sept. 1999.
10. Karimabadi, S. S., Y. Mohsenzadeh, A. R. Attari, and S. M. Moghadasi, "Bandwidth enhancement of single-feed circularly polarized equilateral triangular microstrip antenna," *PIERS Proceedings*, Hangzhou, China, 147–150, Mar. 24–28, 2008.
11. Wei, K., J. Y. Li, L. Wang, R. Xu, and Z. J. Xing, "A new technique to design circularly polarized microstrip antenna by fractal defected ground structure," *IEEE Transactions on Antennas and Propagation*, Vol. 65, No. 7, 3721–3725, Jul. 2017.
12. Prajapati, P. R., G. G. K. Murthy, A. Patnaik, and M. V. Kartikeyan, "Design and testing of a compact circularly polarised microstrip antenna with the fractal defected ground structure for L-band applications," *IET Microwaves Antennas & Propagation*, Vol. 9, No. 11, 1179–1185, 2015.
13. Tanaka, T., M. Takahashi, and K. Ito, "Miniaturization of circularly polarized patch antenna using circular sector element," *IEEE International Workshop on Antenna Technology Small Antennas and Novel Metamaterials*, 209–212, 2006.
14. Tiwari, H. and M. Kartikeyan, "A stacked microstrip patch antenna with fractal shaped defects," *Progress In Electromagnetics Research C*, Vol. 14, 185–195, 2010.
15. Gupta, S., S. Patil, C. Dalela, and B. K. Kanaujia, "Analysis and design of inclined fractal defected ground-based circularly polarized antenna for CA-band applications," *International Journal of Microwave and Wireless Technologies*, Vol. 13, No. 4, 397–406, 2021.
16. Radhakrishnan, R. and S. Gupta, "Axial ratio tuned circularly polarized slot-loaded antenna for S-band and C-band applications," *Progress In Electromagnetics Research C*, Vol. 113, 239–249, 2021.
17. Gupta, S., B. K. Kanaujia, C. Dalela, and S. Patil, "Design of circularly polarized antenna using inclined fractal defected ground structure for S-band applications," *Electromagnetics*, 1–15, 2020.

18. Ambekar, A. G., A. A. Deshmukh, and V. A. P. Chavali, "Investigation into circular polarized response of square microstrip antenna using defected ground structure," *International Conference on Communication information and Computing Technology (ICCICT)*, 2021.
19. Tang, X., Z. Yao, Y. Li, W. Zong, G. Liu, and F. Shan, "A high performance UWB MIMO antenna with defected ground structure and U-shape branches," *International Journal of RF and Microwave Computer-Aided Engineering*, Vol. 2, 21, 2020.
20. Wei, K., B. Zhu, and M. Tao, "The circular polarization diversity antennas achieved by a fractal defected ground structure," *IEEE Access*, Vol. 7, 92030–92036, 2019.
21. Baharuddin, M., V. Wissan, J. T. Sri Sumantyo, and H. Kuze, "Equilateral triangular microstrip antenna for circularly-polarized synthetic aperture radar," *Progress In Electromagnetics Research C*, Vol. 8, 107–120, 2009.
22. Deshmukh, A. A. and K. P. Ray, "Circularly polarized designs of modified isosceles triangular microstrip antennas," *Engineering Reports*, Vol. 2, No. 10, Jun. 2020.
23. Ansys HFSS version 2020 R1.
24. Reddy, V. V. and N. V. S. N. Sarma, "Compact circularly polarized asymmetrical fractal boundary microstrip antenna for wireless applications," *IEEE Antennas and Wireless Propagation Letters*, Vol. 13, 118–121, 2014.
25. Pandey, S. K., G. P. Pandey, and P. M. Sarun, "Circularly polarized microstrip antenna with fractal trees loaded ground plane," *Electromagnetics*, Vol. 39, No. 7, 505–523, 2019.
26. Zhang, Z.-L., K. Wei, J. Xie, J.-Y. Li, and L. Wang, "The new C-shaped parasitic strip for the single-feed Circularly Polarized (CP) microstrip antenna design," *International Journal of Antennas and Propagation*, Vol. 2019, 2019.
27. Wei, K., J.-L. Wang, R. Xu, and X. Ai, "A new periodic fractal parasitic structure to design the circularly polarized microstrip antenna for the satellite navigation system," *IET Microwaves Antennas and Propagation*, Vol. 15, No. 15, 1891–1898, 2021.
28. Samsuzzaman Md., I. and T. Mohammad, "Circularly polarized broadband printed antenna for wireless applications," *Sensors*, Vol. 18, No. 12, 4261, 2018.
29. Singh, M. P., R. K. Jaiswal, K. V. Srivastava, and S. Ghosh, "A miniaturized triple-band circularly polarized antenna using meander geometry," *Journal of Electromagnetic Waves and Applications*, Vol. 36, No. 2, 286–236, 2022.